JOURNAL OF SOLID STATE CHEMISTRY **130,** 176–183 (1997)
ARTICLE NO. SC967265

# An X-Ray and Electron Diffraction Study of the Tetragonal Lead Tungsten Bronze $Pb_{0.26}WO_3$

S. T. Triantafyllou,* P. C. Christidis,*,[1] and Ch. B. Lioutas†

* *Laboratory of Applied Physics, Aristotle University of Thessaloniki, 54006 Thessaloniki, Greece; and*
† *Department of Solid State Physics, Aristotle University of Thessaloniki, 54006 Thessaloniki, Greece*

Received July 8, 1996; in revised form December 11, 1996; accepted December 17, 1996

**The average structure of the tetragonal lead tungsten bronze, $Pb_{0.26}WO_3$, has been determined by single-crystal X-ray diffraction (*P4/mbm* space group, $a_{av} = 12.217(1)$ Å, $c_{av} = 3.7828(7)$ Å and $Z = 10$). The structure refinement based on 370 observed unique reflections (2539 totally measured reflections) with $F_o > 4\sigma(F_o)$ converged to $R = 0.035$ ($R_w = 0.031$). All but one of the oxygen atoms exhibit a twofold disorder. The lead atoms are distributed over three, symmetrically independent, positions inside the pentagonal tunnels. Electron diffraction observations recognize the X-ray average structure. Furthermore, satellite spots appear on the ED patterns revealing a modulated structure, which may be described in terms of a periodic repetition of antiphase boundary planes inside a superstructure related to the average structure by $a_s = \sqrt{2}a_{av}$ and $c_s = 2c_{av}$. The repetition distance is $d = 5/2a_s$ and the displacement vector is $R = 1/2\ a_{av}$.** © 1997 Academic Press

## 1. INTRODUCTION

The tungsten bronzes are ternary nonstoichiometric oxides of the general formula $M_xWO_3$ ($0 < x < 1$), where $M$ is an electropositive element or group. They can be broadly devided into four distinct structural types, the perovskite type (PTB), the tetragonal tungsten bronze type (TTB), the hexagonal tungsten bronze type (HTB), and the intergrowth tungsten bronzes (ITB). Although the main features of the above structural types have been established long ago (1, 2, 3, 4), many of the related compounds have been reanalyzed using modern crystallographic techniques in view of the difficulties, which these compounds often present for an accurate structure determination. The lead tungsten bronzes, $Pb_xWO_3$, were first prepared and studied by Bernoff and Conroy (5). These authors established the existence of a TTB phase in the composition range $0.16 < x < 0.35$, while in the region with lower lead content they observed a gradual transition of the symmetry from pseudotetragonal to monoclinic. Ekström and Tilley (6) performed a new investigation of the Pb–W–O system, primarily in the region of low lead content, where different structure types have been observed in a number of related systems. Their results were in broad agreement with those of Bernoff and Conroy when the preparations of the samples were made at 1373 K. At lower temperatures, however, they established the formation of a series of orthorhombic intergrowth phases (ITB). These phases were formed in samples of overall composition $0.01 < x < 0.18$, although the composition range, over which they were observed alone, was much smaller ($0.03 < x < 0.05$). A more recent study by Dobson *et al.* (7) performed on a sample of composition $Pb_{0.04}WO_3$ confirmed the ITB structure type of this phase. While the lead ITB phases have been studied extensively, considerably less attention has been paid to the lead TTB phase, for which only the cell constants were available (5). Since different variants of the basic TTB structure have been observed in certain tungsten bronzes and other related compounds with some of them exhibiting characteristic superstructures (8, 9), we thought it of interest to carry out a detailed structure investigation on the tetragonal phase of $Pb_xWO_3$ by both X-ray and electron diffraction methods.

## 2. EXPERIMENTAL

Single crystals of the tetragonal lead tungsten bronze were grown by thoroughly mixing Pb and $WO_3$ (Aldrich, 99 + %) in amounts corresponding to the overall composition $Pb_{0.28}WO_3$. The mixture was pressed into tablets and heated in a sealed evacuated silica tube at 1373 K for 7 days, at which point the furnace was turned off and the sample was left to cool. The obtained crystals were of prismatic habit elongated along the $c$ axis. They were dark blue in color and opaque under the optical microscope even for the thinest fragments.

Powder X-ray diffraction patterns were obtained with a Philips PW 1050 diffractometer using Cu$K\alpha$ radiation and

[1] To whom correspondence should be addressed.



0022-4596/97 $25.00

Si as external standard. All the observed reflections could be readily indexed on the basis of the cell constants of Bernoff and Conroy (5). No superstructure reflections were detected on the powder patterns. The refined cell constants along with the observed and calculated values of $d$ spacings, the observed intensities, and the indices of the reflections are given in Table 1.

For the single-crystal X-ray diffraction study, a number of crystals were first examined with the Buerger precession method, from which a very small prism of dimensions $0.225 \times 0.03 \times 0.03$ mm was selected for the measurement of intensities. The diffractometer used was a Philips PW 1100, renovated with respect to its electronic equipment and software by the STOE company.

Accurate lattice parameters were obtained by a least-squares fit of the diffractometer $2\theta$ angles of 52 reflections ($30^\circ < 2\theta < 40^\circ$, Mo$K\alpha$). Intensity data were collected for one half of the reciprocal lattice in the region $0^\circ < 2\theta < 45^\circ$ and for one quarter in the region $45^\circ < 2\theta < 55^\circ$, using graphite monochromated Mo$K\alpha$ radiation and a scintillation counter ($2\theta/\omega$ scans; 51 steps/reflection increased for $\alpha_1$–$\alpha_2$ splitting; step width 0.025°, 1–4 sec/step, three standard reflections every 120 min). A total of 2539 reflections (excluding standards) were recorded, which were further corrected for Lorentz and polarization effects. Also an empirical correction for the absorption effect ($\psi$-scans technique) was applied. The only systematic extinctions found were $h0l$ reflections for $h = 2n + 1$ and $0kl$ reflections for $k = 2n + 1$, leading to $P4/mbm$, $P4bm$, and $P\bar{4}b2$ as possible space groups. No superstructure reflections were detected either in the precession photographs or with help of the diffractometer. By merging the symmetry equivalent reflections a set of 396 unique reflections were obtained of which 370 were considered as observed [$F_o > 4\sigma(F_o)$] and included in the ensuing calculations. The agreement factor of the intensities was $R_{int} = 0.066$ ($R_{int} = 0.108$ if no absorption correction was applied). A summary of the crystal data and of the structure refinement results is given in Table 2.

For the crystal structure analysis calculations the XTAL system of programs was used (10). Atomic scattering factors for neutral atoms and anomalous dispersion corrections were taken from Ref. (11). For the structure solution and refinement the space group $P4/mbm$ was initially adopted taking into account that the intensity statistics clearly favored a centrosymmetric space group. After completion of

**TABLE 1**
**Observed and Calculated Values of $d$-Spacings, Observed Intensities, and Reflection Indices for $Pb_{0.26}WO_3$**
**[$a = 12.2041(6)$Å, $c = 3.7791(4)$Å]**

| $d_{obs}$ | $d_{cal}$ | $I_{obs}$ | $h$ | $k$ | $l$ | $d_{obs}$ | $d_{cal}$ | $I_{obs}$ | $h$ | $k$ | $l$ |
|---|---|---|---|---|---|---|---|---|---|---|---|
| 8.598 | 8.630 | 10 | 1 | 1 | 0 | 1.818 | 1.819 | 17 | 6 | 3 | 0 |
| 6.087 | 6.102 | 4 | 2 | 0 | 0 | 1.791 | 1.791 | 5 | 6 | 0 | 1 |
| 5.440 | 5.458 | 4 | 2 | 1 | 0 | 1.787 | 1.786 | 4 | 2 | 1 | 2 |
| 4.308 | 4.315 | 10 | 2 | 2 | 0 | 1.287 | 1.287 | 3 | 9 | 3 | 0 |
| 3.854 | 3.860 | 59 | 3 | 1 | 0 | 1.275 | 1.274 | 6 | 5 | 5 | 2 |
| 3.776 | 3.779 | 31 | 0 | 0 | 1 | 1.260 | 1.261 | 3 | 6 | 4 | 2 |
| 3.381 | 3.385 | 69 | 3 | 2 | 0 | 1.239 | 1.239 | 8 | 9 | 4 | 0 |
| 3.213 | 3.213 | 6 | 2 | 0 | 1 | 1.233 | 1.233 | 3 | 7 | 7 | 0 |
| 3.106 | 3.107 | 20 | 2 | 1 | 1 | 1.228 | 1.227 | 4 | 2 | 1 | 3 |
| 3.047 | 3.051 | 5 | 4 | 0 | 0 | 1.221 | 1.220 | 5 | 8 | 6 | 0 |
| 2.958 | 2.960 | 100 | 4 | 1 | 0 | 1.218 | 1.218 | 4 | 9 | 3 | 1 |
| 2.874 | 2.877 | 37 | 3 | 3 | 0 | 1.214 | 1.214 | 3 | 10 | 1 | 0 |
| 2.840 | 2.843 | 6 | 2 | 2 | 1 | 1.198 | 1.197 | 4 | 3 | 1 | 3 |
| 2.727 | 2.729 | 33 | 4 | 2 | 0 | 1.178 | 1.178 | 5 | 9 | 4 | 1 |
| 2.698 | 2.700 | 24 | 3 | 1 | 1 | 1.172 | 1.172 | 3 | 7 | 7 | 1 |
| 2.520 | 2.521 | 12 | 3 | 2 | 1 | 1.169 | 1.169 | 3 | 10 | 3 | 0 |
| 2.438 | 2.441 | 4 | 4 | 3 | 0 | 1.166 | 1.165 | 3 | 8 | 2 | 2 |
| 2.372 | 2.374 | 5 | 4 | 0 | 1 | 1.162 | 1.161 | 5 | 8 | 6 | 1 |
| 2.329 | 2.330 | 4 | 4 | 1 | 1 | 1.159 | 1.159 | 4 | 4 | 1 | 3 |
| 2.266 | 2.266 | 4 | 5 | 2 | 0 | 1.157 | 1.156 | 4 | 10 | 1 | 1 |
| 2.211 | 2.212 | 5 | 4 | 2 | 1 | 1.154 | 1.154 | 3 | 3 | 3 | 3 |
| 2.156 | 2.158 | 3 | 4 | 4 | 0 | 1.148 | 1.148 | 3 | 8 | 7 | 0 |
| 2.092 | 2.093 | 10 | 5 | 3 | 0 | 1.141 | 1.141 | 3 | 10 | 2 | 1 |
| 2.050 | 2.050 | 3 | 4 | 3 | 1 | 1.140 | 1.139 | 3 | 8 | 3 | 2 |
| 1.943 | 1.944 | 4 | 5 | 2 | 1 | 1.131 | 1.131 | 4 | 9 | 5 | 1 |
| 1.929 | 1.930 | 38 | 6 | 2 | 0 | 1.129 | 1.128 | 4 | 9 | 6 | 0 |
| 1.889 | 1.889 | 16 | 0 | 0 | 2 | 1.092 | 1.092 | 5 | 10 | 5 | 0 |

**TABLE 2**
**Summary of Crystal Data, X-Ray Measurements, and Structure Refinement Results for $Pb_{0.26}WO_3$**

| | |
|---|---|
| Space group | *P*4/*mbm* (No. 127) |
| *a* (Å) | 12.217(1) |
| *c* (Å) | 3.7828(7) |
| *V* (Å$^3$) | 564.6(1) |
| *Z* | 10 |
| Formula weight | 285.72 |
| *F*(000) | 1193.20 |
| $\rho_{cal}$ (gr·cm$^{-3}$) | 8.403 |
| $\mu$ (Mo$K\alpha$) (cm$^{-1}$) | 727.5 |
| Crystal dimensions (mm) | $0.225 \times 0.03 \times 0.03$ |
| Extinction coefficient (*g*) (Ref. 12) | $2.8(6) \times 10^{-5}$ |
| Measured reflections | 2539 |
| Unique data set | 396 |
| Data with $F_o > 4\sigma(F_o)$ | 370 |
| Transmission factors (Ψ-scans) | 0.022–0.056 |
| $R^a$ | 0.035 |
| $R_w{}^b$ | 0.031 |
| $S^c$ | 1.218 |

[a] $R = \sum||F_o| - |F_c||/\sum|F_o|$.
[b] $R_w = [\sum w(|F_o| - |F_c|)^2/\sum w|F_o|^2]^{1/2}$.
[c] $S = [\sum w(|F_o| - |F_c|)^2/(N_{ref} - N_{param})]^{1/2}$.

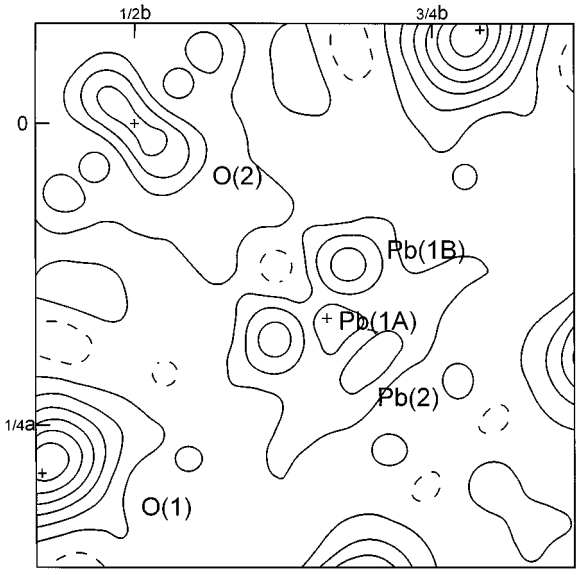


**FIG. 1.** Difference Fourier section at $z = 0$ computed with only the atoms W(1), W(2), and Pb(1*A*). Contours are drawn at 2 eÅ$^{-3}$ intervals. The small crosses on the O(1) and O(2) peaks represent the projected positions of the W(1) and W(2) atoms, respectively. Note the considerable elongation of the O(2) peak along the [110] direction.

the least-squares refinement in *P*4/*mbm* (*vide infra*) the acentric space groups *P*4*bm* and $P\bar{4}b2$ were also tested. Although these refinements yielded slightly improved *R* values, they led either to unacceptable W–O distances or to large variations of the O–W–O angles in the $WO_6$ octahedra. Hence, the space group *P*4/*mbm* was retained as the most probable one for the average structure. The positions of the tungsten atoms were obtained from a sharpened Patterson map, while the positions of all the rest of the atoms were taken from difference Fourier syntheses. Difference Fourier maps computed with the refined positions of only the tungsten and lead atoms (Fig. 1) revealed great similarity to the corresponding ones of the isostructural $Sn_{0.30}WO_3$ (9) with respect to the splitting of the Pb and O(2) atoms on the plane $z = 0$ and the elongation of the electron density peaks O(3), O(4), and O(5) along the *c* axis. The O(1) peak, however, which in the case of $Sn_{0.30}WO_3$ is fourfold split, in our case appears as a single, almost spherical one. These observations led us to introduce an analogous splitting for the atoms Pb and O(2)–O(5) in the least-squares refinement. The site occupation factors for the Pb atoms were allowed to vary freely, while those of the oxygen atoms were kept fixed and equal to 0.5. In the final stage of refinement (full matrix based on *F*) anisotropic displacement parameters for the W atoms and a weighting scheme of the form $w^{-1} = \sigma^2(F_o) = \sigma^2(F_o)_{statistics} + \sigma^2(F_o)_{mod}$, where the $\sigma^2(F_o)_{mod}$ is the so-called "ignorance factor" (10), were introduced. Moreover, an isotropic extinction correction of the Zachariasen type was applied (12). The refinement results after convergence was reached are given in Table 2. The atomic positions along with the displacement and site occupation parameters are given in Table 3.

The electron diffraction study was performed using finely crushed particles and needles grown on the surface of the bulk material glued on copper grids on a JEOL 120CX microscope operating at 120 kV.

**TABLE 3**
**Atomic Positional, Displacement, and Site Occupation Parameters and Anisotropic Displacement Parameters**

| Atom | *x* | *y* | *z* | *U* | *pp* |
|---|---|---|---|---|---|
| W(1) | 0.07671(4) | 0.20486(4) | 1/2 | 0.0119(2)* | 1.000 |
| W(2) | 0 | 1/2 | 1/2 | 0.0166(3)* | 1.000 |
| Pb(1*A*) | 0.1678(2) | $x + 1/2$ | 0 | 0.0387(6) | 0.551(6) |
| Pb(1*B*) | 0.124(2) | 0.681(2) | 0 | 0.020(3) | 0.031(2) |
| Pb(2) | 0.198(3) | $x + 1/2$ | 0 | 0.044(7) | 0.040(6) |
| O(1) | 0.289(1) | 0.419(2) | 0 | 0.051(5) | 1.000 |
| O(2) | 0.018(1) | $x + 1/2$ | 0 | 0.009(5) | 0.500 |
| O(3) | 0.1532(9) | 0.500(1) | 0.431(3) | 0.011(2) | 0.500 |
| O(4) | 0.4322(9) | 0.3570(8) | 0.453(5) | 0.015(2) | 0.500 |
| O(5) | 0.2855(8) | $x + 1/2$ | 0.457(7) | 0.009(4) | 0.500 |

| Atom | $U_{11}$ | $U_{22}$ | $U_{33}$ | $U_{12}$ | $U_{13}$ | $U_{23}$ |
|---|---|---|---|---|---|---|
| W(1) | 0.0110(4) | 0.0097(4) | 0.0149(4) | 0.0002(2) | 0 | 0 |
| W(2) | 0.0135(4) | 0.0135(4) | 0.0228(6) | 0.0041(3) | 0 | 0 |

*Note.* Values marked with an asterisk denote equivalent isotropic displacement parameters. $U_{eq} = 1/3 \sum_i \sum_j U_{ij} a_i^* a_j^* \mathbf{a}_i \cdot \mathbf{a}_j$.

## 3. RESULTS AND DISCUSSION

### 3.1. The Average X-Ray Structure

For a general description of the TTB structure type the reader is referred to the original paper of Magnéli (2). The structure of the tetragonal lead tungsten bronze can be best compared with that of the tetragonal tin tungsten bronze, $Sn_{0.30}WO_3$, due to the chemical similarity of the inserted ions $Pb^{2+}$ and $Sn^{2+}$. A list of selected interatomic distances and angles is given in Table 4. There are two, symmetrically independent, $WO_6$ octahedra in the structure. The W–O distances in the $W(1)O_6$ octahedron range from 1.87(1) to 1.99(1) Å [$\langle W(1)–O\rangle = 1.93(1)$ Å] and in the $W(2)O_6$ octahedron they range from 1.89(1) to 1.918(2) Å [$\langle W(2)–O\rangle = 1.899(4)$ Å]. The maximum deviation of the O–W–O angles from the ideal value of 90° is 8.82° and 14.58° for the first and the second octahedron, respectively. For comparison, in the tetragonal tin tungsten bronze structure the W–O distances in the $W(1)O_6$ octahedron range from 1.89(2) to 2.02(2) Å [$\langle W(1)–O\rangle = 1.95(1)$ Å] and in the $W(2)O_6$ octahedron they range from 1.92(2) to 1.95(1) Å [$\langle W(2)–O\rangle = 1.93(1)$ Å]. Also, the maximum O–W–O angular deviations from 90° in the first and the second octahedron are 22.76° and 18.77°, respectively.

**TABLE 4**
**Selected Interatomic Distances (Å) and Bond Angles (°) for $Pb_{0.26}WO_3$**

| | | Symmetry | | | Symmetry |
|---|---|---|---|---|---|
| W1–O1 | 1.8936(9) | (1, 2) | Pb1A–O3 | 2.97(1) | (8, 12) |
| –O1 | 1.8936(9) | (1, 4) | –O4 | 3.13(1) | (8, 17) |
| –O3 | 1.99(1) | (1, 2) | –O4 | 3.13(1) | (8, 19) |
| –O3 | 1.99(1) | (1, 6) | –O4 | 3.33(1) | (8, 20) |
| –O4 | 1.87(1) | (1, 2) | –O4 | 3.33(1) | (8, 21) |
| –O4 | 1.87(1) | (1, 6) | –O5 | 2.67(2) | (8, 8) |
| –O4 | 1.93(1) | (1, 7) | –O5 | 2.89(2) | (8, 1) |
| –O4 | 1.93(1) | (1, 15) | O1–W1–O3 | 81.2(6) | (2, 1, 2) |
| –O5 | 1.96(1) | (1, 3) | O1–W1–O3 | 96.2(6) | (2, 1, 6) |
| –O5 | 1.96(1) | (1, 5) | O1–W1–O4 | 85.9(8) | (2, 1, 2) |
| W2–O2 | 1.918(2) | (1, 1) | O1–W1–O4 | 87.0(8) | (2, 1, 15) |
| –O2 | 1.918(2) | (1, 8) | O1–W1–O4 | 96.9(8) | (2, 1, 6) |
| –O2 | 1.918(2) | (1, 9) | O1–W1–O4 | 97.6(8) | (2, 1, 7) |
| –O2 | 1.918(2) | (1, 11) | O1–W1–O5 | 83(1) | (2, 1, 3) |
| –O3 | 1.89(1) | (1, 1) | O1–W1–O5 | 92(1) | (2, 1, 5) |
| –O3 | 1.89(1) | (1, 2) | O3–W1–O4 | 84.1(5) | (2, 1, 15) |
| –O3 | 1.89(1) | (1, 6) | O3–W1–O4 | 85.5(5) | (2, 1, 7) |
| –O3 | 1.89(1) | (1, 10) | O3–W1–O5 | 87.6(5) | (2, 1, 3) |
| –O3 | 1.89(1) | (1, 11) | O3–W1–O5 | 88.8(5) | (2, 1, 5) |
| –O3 | 1.89(1) | (1, 12) | O4–W1–O4 | 92.1(4) | (2, 1, 15) |
| –O3 | 1.89(1) | (1, 13) | O4–W1–O4 | 93.1(4) | (2, 1, 7) |
| –O3 | 1.89(1) | (1, 14) | O4–W1–O5 | 94.0(4) | (2, 1, 3) |
| Pb1A–O1 | 3.12(2) | (8, 16) | O4–W1–O5 | 95.0(4) | (2, 1, 5) |
| –O1 | 3.12(2) | (8, 17) | O2–W2–O3 | 75.4(5) | (1, 1, 1) |
| –O1 | 3.38(2) | (8, 8) | O2–W2–O3 | 88.8(5) | (1, 1, 11) |
| –O1 | 3.38(2) | (8, 10) | O2–W2–O3 | 91.2(6) | (1, 1, 14) |
| –O2 | 2.58(1) | (8, 8) | O2–W2–O3 | 104.6(5) | (1, 1, 13) |
| –O2 | 3.22(1) | (8, 9) | O3–W2–O3 | 88.7(5) | (1, 1, 12) |
| –O3 | 2.62(1) | (8, 8) | O3–W2–O3 | 89.2(5) | (1, 1, 6) |
| –O3 | 2.62(1) | (8, 18) | O3–W2–O3 | 90.8(5) | (1, 1, 10) |
| –O3 | 2.97(1) | (8, 1) | O3–W2–O3 | 91.3(5) | (1, 1, 2) |

Symmetry codes

| | | |
|---|---|---|
| 1: $1/2+x, 1/2-y, 1-z$ | 8: $1/2+x, 1/2-y, -z$ | 15: $x, y, z$ |
| 2: $1-y, x, z$ | 9: $1/2-x, -1/2+y, -z$ | 16: $1-x, -y, z$ |
| 3: $1-x, 1-y, z$ | 10: $y, -x, z$ | 17: $1/2+y, -1/2+x, -z$ |
| 4: $1-y, x, 1+z$ | 11: $1/2-x, -1/2+y, 1-z$ | 18: $y, -x, -z$ |
| 5: $3/2-y, 1/2-x, 1-z$ | 12: $y, -x, 1-z$ | 19: $1-x, -y, -z$ |
| 6: $1-y, x, 1-z$ | 13: $1/2-x, -1/2+y, z$ | 20: $1/2+y, -1/2+x, 1-z$ |
| 7: $x, y, 1-z$ | 14: $1/2+x, 1/2-y, z$ | 21: $1-x, -y, 1-z$ |

In many compounds of the TTB structure type the axes of the $WO_6$ octahedra are not strictly parallel to the $c$ axis, but they form angles whose magnitude relates to the structure distortion. In the present case the inclination angles for the $W(1)O_6$ and $W(2)O_6$ octahedra are 2.79°and 9.50°, respectively. The corresponding values for the $Sn_{0.30}WO_3$ case are 13.03° and 10.76°, respectively.

Concerning the distribution of the Pb atoms, the X-ray study clearly indicates that they occupy exclusively the pentagonal interstitial sites, while the tetragonal and trigonal sites remain empty. The splitting of the Pb atoms over three independent sites in the plane $z = 0$ observed in the difference Fourier synthesis (Fig. 1 and Table 3) is completely analogous to that observed in the case of $Sn_{0.30}WO_3$. However, the magnitude of the refined population parameters differ very much in the two cases [Pb(1*A*), 0.551(6); Pb(1*B*), 0.031(2); Pb(2), 0.040(6) compared to Sn(1A), 0.32(3); Sn(1*B*), 0.06(1); Sn(2), 0.21(2)]. These values imply a composition $Pb_{0.26\pm0.01}WO_3$ and indicate a more pronounced concentration of the Pb atoms over the site (1*A*) than of the Sn atoms over the same site in the tetragonal tin bronze. The displacements of the lead atoms normally to the $c$ axis from the barycenter of the pentagonal site are 0.089(2), 0.61(2), and 0.43(3) Å for the Pb(1*A*), Pb(1*B*) and Pb(2) atoms, respectively. The corresponding values for $Sn_{0.30}WO_3$ are 0.36, 0.77, and 0.58 Å. These displacements have been attributed to the stereoactivity of the $6s^2$ and $5s^2$ lone pairs of the $Pb^{2+}$ and $Sn^{2+}$ ions, respectively (9, 13, 14). From the above considerations it can be concluded that the structure of $Pb_{0.26}WO_3$ is substantially less distorted in comparison with that of $Sn_{0.30}WO_3$, which could explain the absence of detectable X-ray superstructure reflections in the former case.

### 3.2. Electron Diffraction Results

Electron diffraction (ED) observations were performed on needles and on the bulk material grains. From the tilting experiments a tetragonal reciprocal space was deduced for the average structure. The electron diffraction patterns of the main zone axes are shown in Fig. 2. From the pattern along the $[001]_{av}$ zone axis, where the subscript av refers to the average tetragonal cell (Fig. 2a), we deduced the lattice

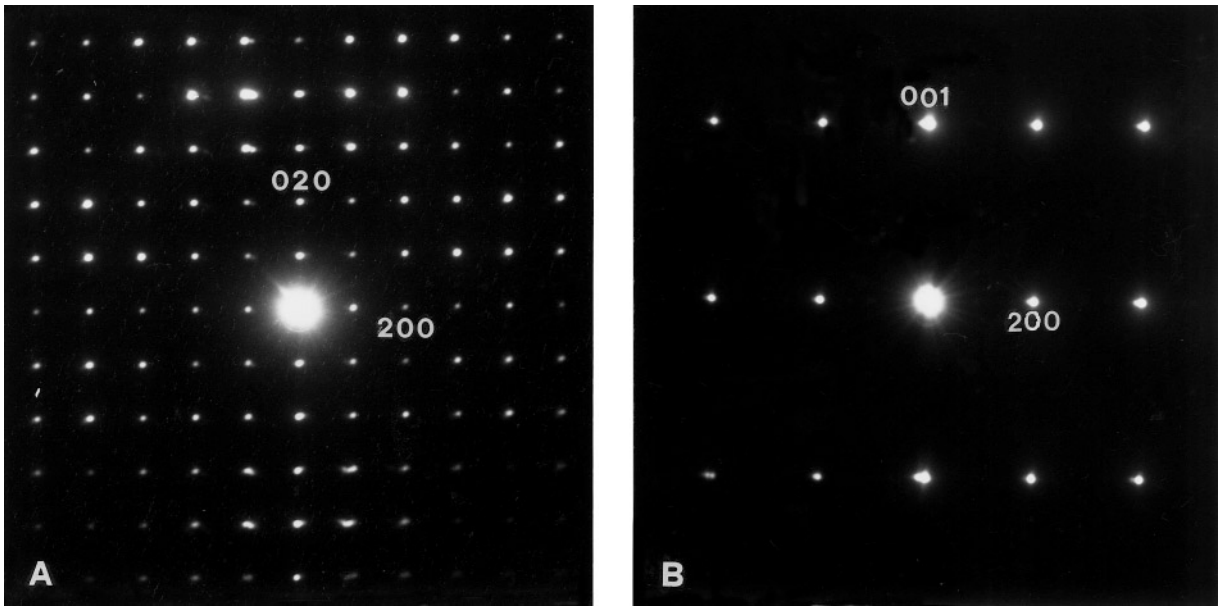


**FIG. 2.** Electron diffraction patterns along (a) $[100]_{av}$ and (b) $[010]_{av}$ zone axes.

parameter $a_{av} = 12.22$ Å in very good agreement with the value found by X-ray diffraction. From the $[010]_{av}$ zone pattern (Fig. 2b) a lattice parameter $c_{av} = 3.75$ Å was obtained, which also compares well with the X-ray results. The same ED pattern confirms the extinction condition $h0l$: $h = 2n + 1$, which is consistent with the space group $P4/mbm$ adopted from the X-ray diffraction study for the average structure. No extra spots were observed in these ED patterns and only inclined sections suggest the existence of a modulated structure.

The most informative ED patterns revealing the modulation features are those containing the $[110]^*_{av}$ row. Figure 3a shows the ED pattern from the $[\bar{1}12]_{av}$ zone. Extra spots appear at rows parallel to the $[110]^*_{av}$ direction

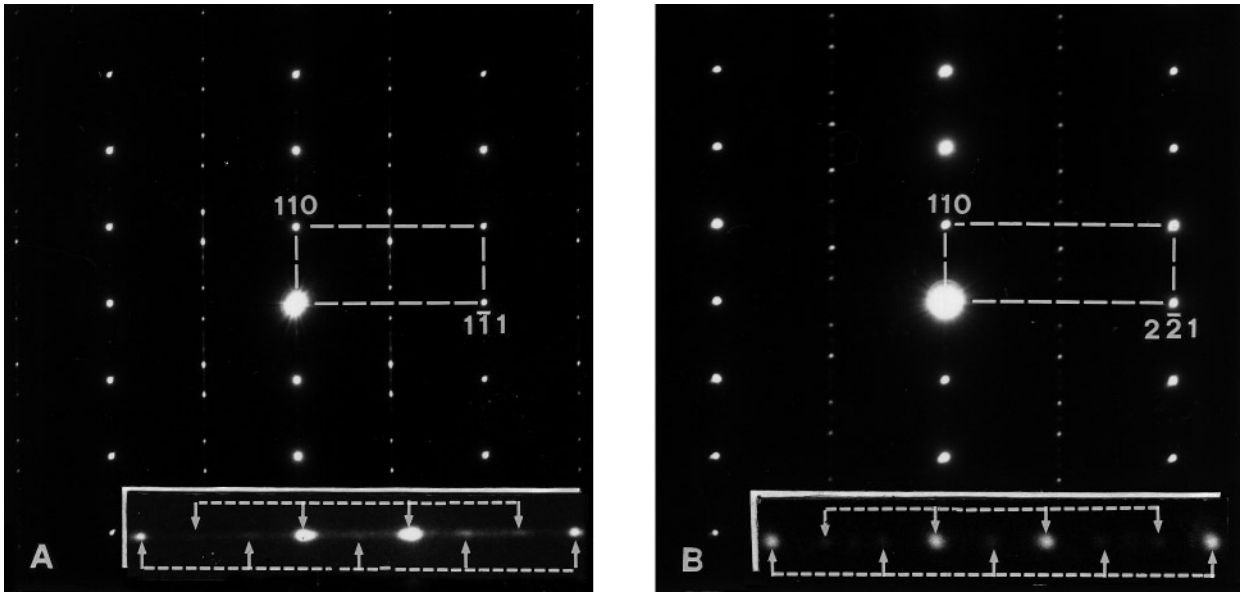


**FIG. 3.** ED patterns revealing the features of the modulated structure: (a) $[\bar{1}12]_{av}$ section and (b) $[\bar{1}14]_{av}$ section. Insets represent enlarged areas around the doublet of the strong superstructure spots. The weak spots with differing distances are interpreted by the overlapping of the satellite spots arrays, which are indicated by the arrows sequence.

and halfway between rows containing exclusively spots from the average structure. Doublets of strong spots are always symmetrically positioned from both sides of the rectangular mesh of the average structure reflections, the separation between successive spots being $2/5\ [110]^*_{av}$. The presence of weak spots with differing distances could be interpreted by the overlapping of the satellite spots arrays (inset in Fig. 3). The ED pattern from the $[\bar{1}14]_{av}$ zone is shown in Fig. 3b. The difference in this case in comparison to the former lies in that the doublets of strong reflections are centered in the rectangular mesh of the average structure reflections. The reciprocal space deduced from these ED patterns is schematically represented in Fig. 4. Series of spots are arranged along the $[110]^*_{av}$ direction with spacing between a doublet of strong superstructure reflections equal to $|\mathbf{u}| = 2/5[110]^*_{av}$. The satellite spot rows are always shifted by a vector $\pm 2/10[110]^*_{av}$ from the fractional positions $h/2$, $k/2$, $l/2$ of the average structure reciprocal space, where $h$, $k$, and $l$ are odd numbers.

### 3.3. *Interpretation of the Electron Diffraction Results as an Interface Modulated Structure*

The features of the observed electron diffraction patterns are typical for interface modulated structures (15). It is well known that a broad class of structures can be interpreted as modulated by the periodic occurrence of translation interfaces. It has been illustrated that it is possible to characterize geometrically this kind of structure from ED patterns by applying the fractional shift method (16, 17). It can be shown that in the kinematical approximation for electron diffraction a periodic modulation in a direction **n** with a period $d$ of translation interfaces and characterized by a displacement vector **R** gives rise to satellite reflections at reciprocal lattice positions **g** given by

$$\mathbf{g} = \mathbf{H} - \frac{\mathbf{n}}{d}(m - \mathbf{H}\cdot\mathbf{R}),$$

where $m$ is an integer and **H** is the reciprocal lattice vector of the corresponding basic structure reflection. From this expression it is clear that the satellite spot rows with interspot distance $|\mathbf{u}| = 1/d$ are shifted over a distance $\mathbf{H}\cdot\mathbf{R}$ with respect to a nonextinct basic structure reflection **H**. In the observed reciprocal space the satellite spots are located in fractional positions of the average unit cell. It is necessary, therefore, to first characterize a superstructure and then use this formalism to interpret the ED results in terms of displaced blocks of the superstructure.

*3.3.1. The possible superstructure.* To find a superstructure model consistent with the observed intensities it is sufficient to consider the sum of the intensities of the strongest satellite spots at the positions around which they are centered (18). From this consideration a tetragonal supercell can be concluded. Furthermore, the absence of any superstructure reflections from the ED patterns of the main zone axes $[100]_{av}$, $[010]_{av}$, and $[001]_{av}$ indicates a body centered unit cell. The relations between the average structure and the superstructure cell parameters are $a_s = \sqrt{2}a_{av}$ and $c_s = 2c_{av}$, where the subscript s stands for superstructure (Fig. 4). It is worth mentioning that in the case of $Sn_{0.30}WO_3$ an analogous superstructure with space group $I4/m$ has been confirmed by X-ray and electron diffraction (9). The occurrence of this superstructure has been interpreted in terms of an ordered arrangement of the axes of all the $WO_6$ octahedra about the $c$ axis. The modulation of the Sn atoms in the pentagonal tunnels has been also proposed as a second reason for the appearance of the superstructure. In the case of $Pb_{0.26}WO_3$ the X-ray analysis revealed a twofold disorder of the apical oxygen atom O(2) in the $W(2)O_6$ octahedron along the directions $\langle 110\rangle$ (*vide supra*). From analogous considerations we may assume that the superstructure of $Pb_{0.26}WO_3$ is due to an ordered arrangement of only the $W(2)O_6$ octahedra about the $c$ axis. Such an arrangement of octahedra within a layer of the structure normal to the $c$ axis is depicted in Fig. 5, where the small arrows indicate the shifts of the O(2) apical atoms from their ideal positions. It should be noted that if the arrows sense in the above arrangement is reversed, the new arrangement is identical to the former after displacing it by the vector $[100]_{av}$. Hence, the stacking of layers of the kind shown in Fig. 5 along the $c$ axis but displaced relative to each other by the vector $[100]_{av}$ gives rise to a body centered supercell and to a doubling of the $c$ axis, while the symmetry is consistent

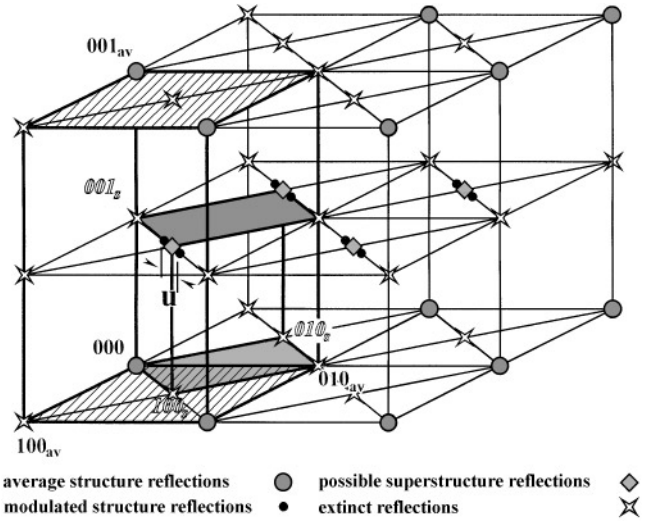


**FIG. 4.** Reconstruction of the reciprocal space obtained from the electron diffraction study. The observed spots are represented by circles. The possible superstructure reflections are indicated by shaded rectangles and they are marked with open letter indices.

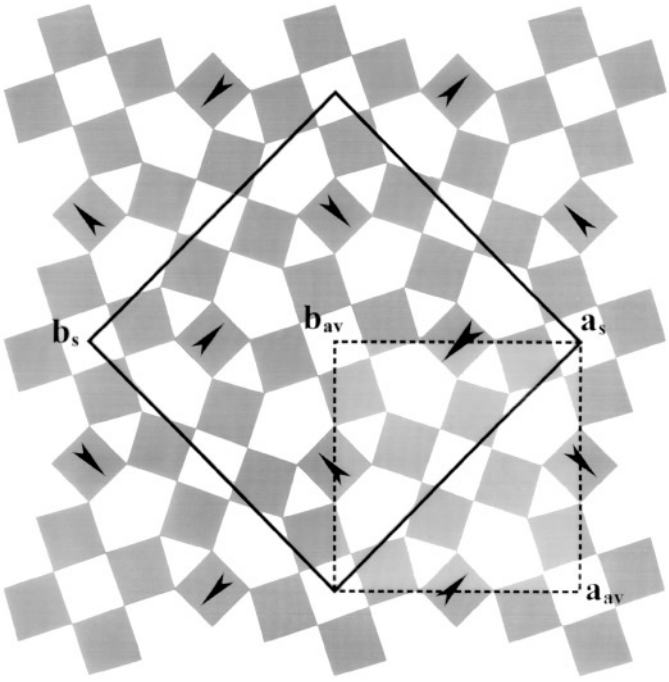


**FIG. 5.** A layer of the structure normal to the *c* axis, showing a possible ordering of the $W(2)O_6$ octahedra. The arrows indicate the inclination sense of the octahedra axes.

with the $I4/m$ space group. Of course, as in the case of $Sn_{0.30}WO_3$, the superstructure can be attributed to an ordering of the lead atoms over the permitted positions in the pentagonal tunnels (*vide supra*), which may be correlated to the ordering of the $WO_6$ octahedra or not.

*3.3.2. The modulated structure.* The ED pattern features can now be interpreted in terms of a planar interface modulated structure. As stated before, the satellite spots are always observed to be arranged parallel to the $[100]^*_s$ direction ($[110]^*_{av}$). Hence, the displacement interfaces are $(100)_s$ planes with a repeat distance $d = 5/2\, a_s$. It was also found that all the satellite spots are shifted from the superstructure reflections positions by the same distance $\pm 2/10 a_s$ or $\pm 2/10\sqrt{2} a_{av}$. Thus, the displacement vector satisfies the condition

$$\frac{\mathbf{n}}{d}(\mathbf{H}\cdot\mathbf{R}) = \pm\frac{2}{10}\mathbf{a}_s \quad \text{or} \quad \mathbf{H}\cdot\mathbf{R} = \frac{1}{2}$$

for all the superstructure reciprocal lattice vectors. It is readily verified that $\mathbf{R} = [\frac{1}{2}\,\frac{1}{2}\,0]_s = [100]_{av}$ or equivalent. The modulated structure arising from a repetition of these antiphase boundaries (APB) for the case of the superstructure model of ordered $WO_6$ octahedra is shown in Fig. 6. The description of the modulated structure on the basis of a superstructure produced by an ordering of the lead atoms in the pentagonal tunnels would be similar.

## REFERENCES

1. M. Atoji and R. E. Rundle, *J. Chem. Phys.* **32,** 627 (1960).
2. A. Magnéli, *Arkiv. Kemi* **1,** 213 (1949).
3. A. Magnéli, *Acta Chem. Scand.* **7,** 315 (1953).
4. A. Hussain and L. Kihlborg, *Acta Crystallogr. A* **32,** 551 (1976).
5. R. A. Bernoff and L. E. Conroy, *J. Am. Chem. Soc.* **82,** 6261 (1960).
6. T. Ekström and R. J. D. Tilley, *J. Solid State Chem.* **24,** 209 (1978).
7. M. M. Dobson, J. L. Hutchison, R. J. D. Tilley, and K. A. Watts, *J. Solid State Chem.* **71,** 47 (1987).
8. F. Takusagawa and R. A. Jacobson, *J. Solid State Chem.* **18,** 163 (1976).
9. M. Goreaud, Ph. Labbé, Y. Monfort, and B. Raveau, *Rev. Chim. Minerale* **17,** 79 (1980).

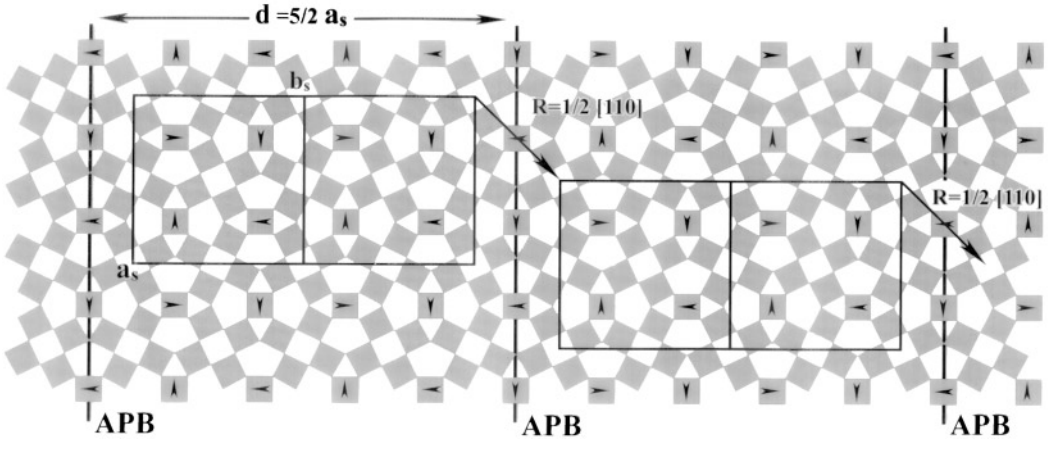


**FIG. 6.** A layer of the modulated structure normal to the *c* axis, based on the ordering of the $WO_6$ octahedra. The superstructure cell and the displacement vector between neighboring blocks separated by an APB are also indicated.

10. S. R. Hall, H. D. Flack, and J. M. Stewart, "XTAL 3.2 Reference Manual." Universities of Western Australia, Geneva and Maryland, 1992.
11. "International Tables for X-Ray Crystallography," Vol. IV, The Kynoch Press, Birmingham, 1974.
12. W. H. Zachariasen, *Acta Crystallogr.* **23,** 558 (1967).
13. Ph. Labbé, M. Frey, B. Raveau, and J. C. Monier, *Acta Crystallogr. B* **33**, 2201 (1977).
14. M. Goreaud, Ph. Labbé, and B. Raveau, *Acta Crystallogr. B* **36,** 19 (1960).
15. J. Van Landuyt, R. De Ridder, and S. Amelinckx, *Mater. Res. Bull.* **5,** 353 (1970).
16. R. De Ridder, J. Van Landuyt, and S. Amelinckx, *Phys. Stat. Sol.* (*a*) **9,** 551 (1972).
17. D. Van Dyck, D Broddin, J. Mahy, and S. Amelinckx, *Phys. Stat. Sol.* (*a*) **103,** 357 (1987).
18. R. Deblieck, J. Van Landuyt, D. Van Dyck, G. Van Tendeloo, and S. Amelinckx, *J. Solid State Chem.* **70,** 108 (1987)